Published in final edited form as:
Neuroimage. 2010 February 1; 49(3): 2467. doi:10.1016/j.neuroimage.2009.09.054.

Interhemispheric neuroplasticity following limb deafferentation detected by resting-state functional connectivity magnetic resonance imaging (fcMRI) and functional magnetic resonance imaging (fMRI)

Christopher P. Pawela[a,d], **Bharat B. Biswal**[b], **Anthony G. Hudetz**[c], **Rupeng Li**[a], **Seth R. Jones**[d], **Younghoon R. Cho**[d], **Hani S. Matloub**[d], and **James S. Hyde**[a,*]

[a] Department of Biophysics, Medical College of Wisconsin, 8701 Watertown Plank Road, Milwaukee, WI 53226, USA

[b] Department of Radiology, UMDNJ New Jersey Medical School, ADMC Building 5, Suite 575, 30 Bergen Street, Newark, NJ 07103, USA

[c] Department of Anesthesiology, Medical College of Wisconsin, 8701 Watertown Plank Road, Milwaukee, WI 53226, USA

[d] Department of Plastic Surgery, Medical College of Wisconsin, 8701 Watertown Plank Road, Milwaukee, WI 53226, USA

Abstract

Functional connectivity magnetic resonance imaging (fcMRI) studies in rat brain show brain reorganization following peripheral nerve injury. Subacute neuroplasticity was observed two weeks following transection of the four major nerves of the brachial plexus. Direct functional magnetic resonance imaging (fMRI) stimulation of the intact radial nerve reveals an activation pattern in the forelimb regions of the sensory and motor cortices that is significantly different from that observed in normal rats. Results of this fMRI experiment were used to determine seed voxel regions for fcMRI analysis. Intrahemispheric connectivities in the sensorimotor forelimb representations in *both* hemispheres are largely unaffected by deafferentation, whereas substantial disruption of interhemispheric sensorimotor cortical connectivity occurs. In addition, significant intra- and interhemispheric changes in connectivities of thalamic nuclei were found. These are the central findings of the study. They could not have been obtained from fMRI studies alone—both fMRI and fcMRI are needed. The combination provides a general marker for brain plasticity. The rat visual system was studied in the same animals as a control. No neuroplastic changes in connectivities were found in the primary visual cortex upon forelimb deafferentation. Differences were noted in regions responsible for processing multisensory visual-motor information. This incidental discovery is considered to be significant. It may provide insight into phantom limb epiphenomena.

Introduction

In this paper, functional connectivity magnetic resonance imaging (fcMRI), which is based on a series of images acquired at rest, was applied to the study of neuroplasticity in adult deafferented rats. Recently, fMRI has been applied to the study of brain plasticity in rat models

*Corresponding Author: James S. Hyde, Ph.D., Department of Biophysics, Medical College of Wisconsin, 8701 Watertown Plank Road, Milwaukee, WI 53226, Phone: 414-456-4005, Fax: 414-456-6512, E-mail: jshyde@mcw.edu.

(Endo et al. 2007; Pelled et al. 2006; Ramu et al. 2007; Weber et al. 2008). Experience or brain damage/recovery has been shown to cause task-related changes in the blood oxygen level dependent (BOLD) fMRI signal. Plasticity can be a consequence of normal brain activity, as in the case of repetition of learned motor task (Karni et al. 1995), or lesional, as in the case of stroke (Feydy et al. 2002). These studies (Feydy et al. 2002; Karni et al. 1995) document changes to the task-activated brain network, but little is known about changes in the resting-state brain network. Rats in the present study underwent a surgical procedure that denervated a single forepaw and then were allowed to recover. The rats were scanned two weeks post recovery using BOLD resting-state fMRI/fcMRI and analyzed for neuroplastic changes. The hypothesis was tested that loss of afferent input from the damaged limb causes detectable changes in the activated, as well as the resting, brain.

Correlations in the low-frequency fluctuations (LFFs) of the resting-state BOLD signal were originally discovered between both hemispheres of the human motor cortex (Biswal et al. 1995). This original observation of correlations in BOLD LFFs between brain regions has now been extended to monkeys (Shmuel and Leopold 2008; Vincent et al. 2007) and rats (Kannurpatti et al. 2008; Lu et al. 2007; Pawela et al. 2008; Zhao et al. 2008). Spontaneous neuronal activity has been implicated as the basis for BOLD LFFs (Biswal et al. 1995; Lu et al. 2007). Resting-state fcMRI has been used in the diagnosis of a variety of diseases including schizophrenia (Fox and Raichle 2007; Liu et al. 2008) and Alzheimer's disease (Li et al. 2002; Sorg et al. 2007). Recently, resting-state connectivities have been shown to be disrupted in regions of the visual system in blind subjects when compared to sighted controls (Liu et al. 2007). In the present work, evidence is presented that severe injury in the peripheral nervous system causes disruption in the correlations of BOLD LFFs between regions of the sensorimotor system.

Electrophysiology has been the major technique used in the examination of cortical plasticity (Merzenich et al. 1983a; Merzenich et al. 1983b; Wall and Cusick 1984). This technique has excellent utility for the localization of neuronal activity but is very invasive and has spatial limitations. Limb deafferentation has been studied using electrophysiological techniques in rats (Donoghue and Sanes 1987; Wall and Cusick 1984) and other animal models (Kalaska and Pomeranz 1979; Pons et al. 1991). Reorganization occurs in both the motor (Donoghue and Sanes 1987; Donoghue and Sanes 1988; Sanes et al. 1990) and sensory cortices (Pearson et al. 2003; Pluto et al. 2005; Wall and Cusick 1986) in response to limb amputation. This neuroplasticity occurs within hours (Sanes et al. 1988), days (Wall and Cusick 1984), or weeks (Pearson et al. 2003) following injury. Functional MRI and fcMRI are noninvasive methods and can be used to track global brain neurophysiological changes. In the present study, both fMRI and fcMRI were used to examine the task-activated and resting sensorimotor system after complete forepaw denervation. The resting-state visual system of the rat was used as a control because it was hypothesized that forelimb deafferentation would cause little change to this sensory brain network within the two-week recovery period.

It has been hypothesized that the task-activated network is a subset of the resting-state network (Fox and Raichle 2007; Greicius et al. 2003; Raichle and Snyder 2007; Xiong et al. 1999). Functional connectivity MRI may have utility over fMRI in studies in which the task does not excite the entire network or performance of task is difficult. However, comparison of BOLD task-activation maps and resting-state functional imaging results is a natural pairing. The purpose of the current work is to investigate neuroplastic changes that occur in the activated and resting rat brain in response to surgical forelimb denervation and to test specific hypotheses about the combined application of fMRI and fcMRI to brain plasticity. This study reveals brain intra- and interhemispheric changes in the sensorimotor resting-state connectivities in reaction to peripheral nerve injury.

Materials and Methods

General methods

All protocols and procedures were carried out in compliance with federal regulations and guidelines of the Medical College of Wisconsin's Institutional Animal Care and Use Committee (IACUC). Six Sprague-Dawley rats (Charles River Laboratories, Wilmington, MA, USA) (300–400 g) underwent a procedure that denervated the right forepaw followed by fMRI and fcMRI studies of the visual and sensorimotor systems. Six Sprague-Dawley rats were used as a control in the study of BOLD fMRI activation in response to forepaw and radial nerve stimulation. Twenty healthy Sprague-Dawley rats (Charles River Laboratories, Wilmington, MA, USA) (300–400 g) were used as a control in the fcMRI sensorimotor system experiments, and 15 healthy Sprague-Dawley rats (Charles River Laboratories, Wilmington, MA, USA) (300–400 g) were used as a control in the study of the visual system.

Denervation procedure and recovery

Rats were initially anesthetized with 2.5% isoflurane (Halocarbon Laboratories, River Edge, New Jersey, USA) and placed supine on a heated surgical table. Isoflurane anesthesia was reduced to 1.5% for maintenance. An incision was made along the medial aspect of the right upper extremity. The subcutaneous tissues were retracted, and the pectoralis major muscle identified and extended into the axilla and a portion of the flank. The pectoralis was retracted medially to expose the brachial plexus and artery. There are four major nerves of the brachial plexus: median, ulnar, radial, and musculocutaneous. The largest and most visible nerve is the median. The ulnar nerve resides parallel and medial to the median nerve. The radial nerve lies deep to the brachial artery. The long and short heads of the biceps brachii are lateral to the major neurovascular bundle. The long head of the biceps brachii was reflected laterally, exposing the musculocutaneous nerve between the retracted biceps muscles. All four major nerves in the right forelimb (median, ulnar, radial, and musculocutaneous) were surgically transected. A section of each nerve was completely removed to prevent reattachment. The initial incision was then sutured and the animal was allowed to recover. Buprenorphine (0.05 mg/kg) was injected subcutaneously every 12 hours for two days for pain management. A quarter section of a 100 mg tramadol pill (ULTRAM, ORTHO-McNEIL, Titusville, NJ, USA) was crushed and added to a small amount of fruit-flavored Jell-O for treatment of phantom limb pain. The Jell-O mixture was fed to the rat each day during the recovery period. A two-week period was allowed between the denervation procedure and the scanning session. No signs of self-mutilation were found during the recuperation phase.

Surgical protocol prior to fMRI/fcMRI experiments

All rats in this study underwent a pre-imaging surgical protocol. Subject rats were removed from caging and placed in a gas anesthesia box. Isoflurane was started at 2.5% and the rat anesthetized. The rat was then placed on a heated surgical table and isoflurane continued at 1.5%. The right femoral vein was cannulated for experimental access with PE-50 tubing (Stoelting, Wood Dale, IL, USA). A tracheostomy was performed for mechanical ventilation during the fMRI protocol. Both incisions were carefully sutured, and the subject rat was placed on a custom-built, heated G-10 fiberglass rodent cradle for imaging. G-10 was used because it has a magnetic susceptibility similar to air. Animal temperature was maintained at 37°C by a recirculating water pump (Meditherm-III, Gaymar Industries, Orchard Park, NY, USA). An intravenous infusion mixture of 100 μg/kg/hr medetomidine hydrochloride (Domitor, Pfizer Animal Health, New York, NY, USA) and 2 mg/kg/hr pancuronium bromide (Hospira, Lake Forest, IL, USA) was started and isoflurane anesthesia ended. Infusion was possible in the MRI environment with the use of an MRI-compatible infusion pump (PHD 2200, Harvard Apparatus, Boston, MA, USA). Bipolar copper-beryllium electrodes were placed between the webspaces of the second and fifth digits of each forepaw.

Electrode implantation

During the pre-imaging surgery, the six denervated and six control rats underwent an additional protocol that implanted an electrode on the left radial nerve. An incision was made along the median aspect of the left upper forelimb and the brachial plexus nerves exposed. A 150 μm electrode (Plastics One, Roanoke, VA, USA) was attached to the radial nerve and the incision closed with nylon suture. A shielded MRI-compatible cable was attached from the electrode to the electrical stimulator outside the scanner.

fcMRI/fMRI parameters

A 9.4 T small-animal scanner (AVANCE, Bruker, Billerica, MA, USA) was used for all imaging procedures. A surface receive coil (T9208, Bruker, Billerica, MA, USA) and a linear transmit coil (T10325, Bruker, Billerica, MA, USA) were employed during the fcMRI/fMRI protocol. A rapid acquisition with relaxation enhancement (RARE) anatomic image was obtained prior to each fcMRI or fMRI experiment. For the sensorimotor system, RARE parameters were TR = 2.5 sec, TE = 50.8 ms, FOV = 35 mm, and 256 × 256 matrix. Ten 1-mm-thick contiguous slices were acquired, with the third slice located directly over the anterior commissure (−0.36 mm from bregma). For the visual system, RARE parameters were TR = 2.5 sec, TE = 50.8 ms, FOV = 35 mm, and 256 × 256 matrix. Fifteen 1-mm-thick contiguous slices were acquired, with the third slice located directly over the anterior commissure (−0.36 mm from bregma). Two resting-state fcMRI acquisitions were performed prior to each stimulation fMRI experiment. T2*-weighted echo-planar imaging (EPI) sequences were used for all fMRI/fcMRI experiments. EPI parameters for both task-activation and resting-state scans were TR = 2 sec, TE = 18.76 ms, FOV = 35 mm, 96 × 96 matrix (zero filled to 128 × 128 matrix), with the same slice geometry as the RARE images. 110 images were obtained during each fcMRI/fMRI experiment for a total acquisition time of 3 min 40 sec.

fMRI electrical stimulation method

A square-wave electrical generator (S88, Grass Telefactor, Warrick, RI, USA) equipped with a constant-current power supply (CCU, Grass Telefactor, Warrick, RI, USA) was used for stimulation. A standard block design stimulation protocol of 40 sec rest followed by three periods of 20 sec ON and 40 sec OFF was used (total of 3 min 40 sec). Electrical stimulation was computer-controlled and triggered by a transistor-transistor logic (TTL) pulse from the scanner. The forepaw was stimulated with square-wave pulses at 10 Hz frequency, 3 ms pulse width, and 2 mA amplitude, and the radial nerve stimulated at 5 Hz frequency, 1 ms pulse width, and 1 mA amplitude. Two stimulation fMRI experiments were performed for each condition for a total of four fMRI acquisitions.

fMRI visual stimulation method

Blue, MRI-compatible light-emitting diodes (LEDs) with a wavelength of 465 nm were placed bilaterally 2 cm from the eyes of the rat. The LEDs were computer-controlled (Labview Software, National Instruments, Austin, Texas, USA) and triggered by a TTL pulse from the scanner. The lights in the scanner suite were turned off. The same boxcar stimulation sequence used for the forepaw was used for visual stimulation. Light activation was used as an internal control. The BOLD activation patterns in response to visual stimulation were in good agreement with our earlier work (Pawela et al. 2008).

Physiological monitoring during MRI acquisition

Several physiological parameters were continuously monitored during all imaging experiments. These included pulse oximetry (Model 8600 V, Nonin Medical, Plymouth, MN, USA), chest respiration (Model 1025, SA Instruments, Stony Brook, NY, USA), and end tidal gases (POET IQ2, Criticare Systems, Waukesha, WI, USA). The subject rat was mechanically

ventilated using an MRI-compatible ventilator (MRI-1, CWE, Ardmore, PA, USA) with a 30/70 O_2/N_2 inhalation gas mixture. The respiratory rate was maintained between 55 and 65 breaths per minute. Respiratory parameters were adjusted to maintain physiologic parameters in normal ranges.

fMRI data analysis

All EPI acquisitions were registered to an "ideal" RARE image using the Oxford Center for Functional Magnetic Resonance of the Brain's (FMRIB) Linear Image Registration Tool (FLIRT) program (Jenkinson and Smith 2001). The "ideal" RARE image was chosen to have the best gray-white contrast from the entire experimental subset. Further analysis was done using the program Analysis of Functional Neuroimages (AFNI) (Cox and Hyde 1997). The registered EPI acquisitions were averaged using the AFNI 3dcalc program. These averaged EPI datasets were used to create activation maps by performing an F-test on the time series with the block design as the only regressor (AFNI, 3dDeconvolve). A p-value of 0.005 was used for plotting and was the threshold for activation used in the time-course analysis. All activation maps were overlaid on the "ideal" RARE image for display. Time-course analysis was performed by averaging activated voxel time-courses from each specific ROI across every animal.

Regions of interest

Brain regions were drawn on the "ideal" RARE image freehand using AFNI. The Paxinos' stereotactic rat brain atlas (Paxinos 2005) was consulted for accuracy. Regions of interest (ROI) drawn from the sensorimotor region include the primary/secondary motor cortex (M1/M2), the primary sensory forelimb region (S1FL), the primary sensory trunk region (S1Tr), the secondary sensory region (S2), the corpus callosum (CC), the sensorimotor thalamus (SMT), the ventral posterior thalamic nucleus (VP), the posterior thalamic nucleus (VP), the reticular thalamic nucleus (Rt), the caudate putamen (CP), and the globus pallidus (GP). ROIs drawn from the visual system include the primary visual cortex (V1), the secondary visual cortex (V2), the temporal association cortex (TeA), the dorsal lateral geniculate nucleus (DLG), the lateral posterior nucleus (LP), and the superior colliculus. An ROI was also drawn for the rat hippocampus (HIP).

fcMRI seed voxel analysis

Both resting-state fcMRI experiments for each animal were combined to build a new dataset. We used cross-correlation analysis between the average time-courses of six reference voxels at the center of the region chosen from the functional anatomy. Those time-courses were correlated with every other voxel time-course in that slice. Since we are only interested in the temporal correlation due to slow periodic spontaneous oscillations, a finite impulse response filter was used to filter the high-frequency components from each of the datasets. Because of the short data size, filter parameters were adjusted to minimize the generation of artifactual frequencies (sidelobes). All voxels that passed a correlation coefficient threshold of 0.35 were considered significant, and those locations were noted.

fcMRI regional analysis

A regional pairwise correlation coefficient (RPCC) matrix was tabulated using the averaged filtered time-course from each region. The two resting-state fcMRI datasets for each individual animal were combined to create a new, 220-time-point dataset. The new dataset was used in the RPCC analysis. Datasets were first detrended to eliminate linear drifts. A low-pass filter with a cutoff at 0.1 Hz was applied to all regional time-courses. Principal component analysis (PCA) was carried out for each region within the sensorimotor system. Using PCA, a dataset of orthogonal waveforms was determined for each region. Briefly, PCA is a multivariate

technique that replaces the measured variables by a set of principal components arranged in the order of decreasing standard deviation (SD) or energy distribution. For this study, the first two components accounted for more than 75% of the SD for each ROI, and a mixture of the two was therefore used in the RPCC analysis. The resulting time series for each region was correlated with every other regional time component to obtain a pair-wise correlation matrix. The PCA was run independently for each region.

Results

BOLD task-activation studies

Averaged fMRI BOLD activation maps for six rats in response to electrical forepaw stimulation at 10 Hz, 3 ms, 2.0 mA are shown in Fig 1. Figure 1 displays normal healthy rats with stimulation of the left (Fig. 1A) and right (Fig. 1B) forepaw. Figures 1C and 1D show right-limb deafferented rats with stimulation to the healthy left forepaw and stimulation to the denervated right forepaw, respectively. The slice is centered 0.64 mm from bregma. The S1FL region contralateral to the side of forepaw stimulation demonstrates positive BOLD activation in reaction to electrical stimulation of the left paw for both healthy (Fig. 1A) and deafferented (Fig. 1C) rats. No statistical differences in BOLD activation area for S1FL were found compared to stimulation of the healthy forepaw in control animals (182 ± 37 voxels) and stimulation of the left intact paw (166 ± 48 voxels) in denervated animals. Negative BOLD activation is apparent in both sides of the caudate putamen in both healthy (Fig. 1A) and denervated (Fig. 1C) rats. In contrast to the left side, stimulation of the damaged right forepaw in denervated animals caused no task-related BOLD activation (0 ± 0 voxels) (Fig. 1D) in the S1FL region. When comparing BOLD activation to visual stimulation, patterns between normal and deafferented rats revealed no statistically significant differences (unreported data).

Figure 2 displays averaged BOLD activation maps for six rats in response to left limb direct radial nerve stimulation at 5 Hz, 1 ms, 1.0 mA. Healthy control rats are plotted in Figs. 2A,B, and right limb deafferented rats are plotted in Figs. 2C, D. Figures 2A,C exhibit a slice centered 0.64 mm from bregma, and Figs. 2B,D display a slice centered −1.36 mm from bregma. Bilateral S1FL BOLD activation occurs in response to electrical stimulation of the radial nerve for denervated rats. In contrast, healthy rats demonstrate positive BOLD response in the contralateral S1FL and negative BOLD response in the ipsilateral S1FL. Deafferented animals demonstrate positive bilateral BOLD activation in the caudate putamen, VP, S2, and reticular nuclei of the thalamus in response to nerve stimulation. Healthy rats display bilateral negative BOLD in the caudate putamen and S2, and positive contralateral BOLD in the VP and reticular thalamic nuclei. The BOLD activation patterns were consistent across both experimental and control animals. The activation maps present major differences in the task-activated network in response to direct radial nerve stimulation between deafferented and healthy rats.

Figure 3 is a plot of averaged activated BOLD voxel time-courses from three regions of the sensorimotor system for both control and denervated rats in response to radial nerve stimulation at 5 Hz, 1 ms, 1 mA. A single time-course was created by averaging across all three stimulation ON periods. The red line corresponds to the averaged time-courses from control animals. The blue line corresponds to the averaged time-courses from denervated rats. Positive BOLD response is indicated in the contralateral S1FL and the thalamus in control rats. This is in contrast to denervated rats, which display positive response in all regions plotted. Negative BOLD response is observed in the ispilateral S1FL and the ispilateral/contralateral caudate putamen in control animals. No negative BOLD response was evident in the examination of the denervated animal time-courses.

BOLD resting-state LFFs

A seed voxel approach was used to examine resting-state fcMRI data. A seed voxel region was placed in the right S1FL region (side ipsilateral to the right denervated paw in the experimental animals) for both control (Fig. 4A) and deafferented (Fig. 4B) rats. The seed region appears yellow in the fcMRI maps. Robust correlation across voxels over the entire cortex is visible in the control animals (Fig. 4A). Some intrahemispheric cortical correlation is observed in the deafferented animals (Fig. 4B). Weaker interhemispheric correlation is evident in the denervated rats when compared to the healthy controls. To explore both intra- and interhemispheric connectivity further, regional pairwise correlation coefficient matrices were computed.

To determine the effect of baseline noise on the PCA analysis, the first two PCA components from various ROIs were compared to the first two components used from a region outside the brain. This region has scanner noise but no physiological signal. The mean correlation coefficient between the PCA used for the analysis and the PCA from the scanner noise was 0.038. Figure 5 is a power spectrum of a representative PCA regional time-course taken from data (red) and a regional filtered time-course taken from outside the brain (blue). There is a significant reduction in the amplitude of the time-course taken from outside the brain (blue) when compared to the regional time-course (red). Furthermore, the frequency spectrum from the scanner noise is flat, suggesting the absence of any particular frequency.

Known connections between brain regions in the rat are plotted in Fig. 6. The sensorimotor system is shown in Fig. 6A and the visual system in Fig. 6B. These connections were determined by examination of prior histological tract-tracer studies (Paxinos 2004). Resting-state analysis was carried out using these brain regions. This chart has previously been published in our paper on BOLD resting-state connectivity in rats (Pawela et al. 2008) and is reproduced here for convenience.

An RPCC matrix was tabulated for resting-state BOLD LFF correlation coefficients between brain regions (Figs. 7A,B and 8A,B). Figure 7 is the matrix tabulated from regions within the sensorimotor system, and Fig. 8, from regions in the visual system. Averaged data from 20 healthy rats were used to create Figs. 7A, averaged data from a separate group of 15 healthy rats were used to create Fig. 8A, and averaged data from 6 denervated animals were used to create Figs. 7B and 8B. The RPCC matrix is symmetric about the main diagonal. The lower triangular part of the matrix displays a colored plot of the correlations between regions based on the color bar to the right of the figure. The upper triangular part of the matrix contains the corresponding correlation coefficients. Along the main diagonal, each regional time-course is correlated with itself, and, therefore, the entries have a correlation coefficient value of 1.0. Regions with a pairwise correlation above 0.35 are generally considered to be connected (Biswal et al. 1995). A correlation of 0.35 corresponds to an equivalent p-value after correction for temporal smoothness of 0.0016. Located to the right of the RPCC matrices (Figs. 7C and 8C) is a difference matrix resulting from the subtraction of Fig. 7B from 7A (Fig. 7C), and Fig. 8B from 8A (Fig. 8C). These difference matrices highlight regional variation between RPCC matrices. The colors displayed on the lower triangular portion of the difference matrix correspond to the color bar located to the right of the figure. The corresponding difference values are plotted on the upper triangular part of the matrix.

Resting-state sensorimotor system

The RPCC matrix in Fig. 7A shows that the intracortical and intrathalamic regions contain the highest pairwise correlations. Cortico-thalamic connections are also quite strong for healthy rats. All regions are strongly correlated to their regional counterparts on the opposite side of the brain. The superior colliculus (SC) from the visual system is included in Figs. 7A,B as a

control. We hypothesized that most of the regions in the visual system would only be weakly connected to the sensorimotor system and, therefore, should have low correlation. As expected, the visual SC has a low correlation (< 0.30) with the sensorimotor network in healthy animals. These results are in good agreement with our previous study of fcMRI in rats (Pawela et al. 2008). No statistical differences between the two studies were demonstrated when tested with an unpaired t-test with a 95% confidence interval (unreported data).

The RPCC matrix for six denervated animals is displayed in Fig. 7B. To highlight intrahemispheric resting-state connectivity differences, Table 1 of the known brain region connections taken from Fig. 6 was formed and averaged for both brain hemispheres. The sensorimotor connectivities are listed first in Table 1. An unpaired t-test with a 95% confidence interval was used to check for statistical significance in the correlation coefficient values. Only one intrahemispheric connection shows a statistically significant difference between healthy and deafferented animals in the sensorimotor system: left-side S1FL to M1/M2 in deafferented rats (highlighted in gray). The averaged S1FL to M1/M2 correlation coefficient is lower (0.49) when compared to healthy animals (0.82, 0.69) and the right side (0.71) in experimental animals. This connection is contralateral to the right denervated limb. The other regions demonstrated no statistically significant differences.

Disruption in interhemispheric cortical connectivity is demonstrated in Fig. 9. Left-to-right hemispheric cortical connectivities are listed for both healthy and deafferented rats. The interhemispheric correlation coefficients between S1FL, M1/M2, and S2 are displayed. These cortical regions are directly connected from the left-to-right sides through the corpus callosum, as shown in Fig. 6. Statistical significance for correlation coefficients was tested by using an unpaired t-test with a 95% confidence interval. The interhemispheric connectivity is markedly diminished in deafferented rats compared to healthy controls. All correlation coefficients between healthy and experimental rats shown in Fig. 6 were statistically significant when matched pairs were evaluated. Figure 9 demonstrates that the interhemispheric resting-state connectivity is severely disrupted by limb deafferentation within a two-week time frame.

Resting-state visual system

RPCC matrices for the visual system are presented in Figs. 8A,B. The matrix from healthy rats (Fig. 8A) is visually similar to the matrix from rats that received right-forepaw denervation (Fig. 8B). The hippocampus region (HIP) was used as a control because it was believed that this region would be weakly coupled to the visual system. Data from our previous paper on resting-state connectivity in rats (Pawela et al. 2008) were used to generate data for the control animals (Fig. 8A). Again, differences are highlighted in Fig. 8C. Table 1 lists intrahemispheric connectivities from the visual system based on the connections from Fig. 6B. Connections between visual system areas that carry multisensory information demonstrate statistically significant intrahemispheric differences (highlighted in gray) when tested with an unpaired t-test with a 95% confidence interval. These include left-side LP to TeA, right-side LP to V2, and right-side SC to LP.

By examining the difference map in Fig. 8C, interhemispheric connections can be evaluated. The interhemispheric connectivity divergence between the left and right primary visual cortex (V1) is small between control and experimental animals (0.06). The secondary visual cortex (V2) also demonstrates a slight interhemispheric disparity (0.07) between the groups. In contrast to V1, V2, and the DLG, higher order multisensory regions demonstrate larger differences between healthy and deafferented animals. For example, the differences between the left TeA region and the left or right SC are 0.21 and 0.39, respectively; the left TeA region and the left or right LP, 0.22 and 0.17, respectively; and the left LP and the right LP, 0.27. These differences highlight areas that carry multisensory information (TeA/LP) and are shown

to be affected by forelimb deafferentation, whereas visual-system-specific regions (V1/V2) are unaffected.

Multisensory interactions

There are some potentially significant results in the difference maps in the control areas of the sensorimotor RPCC matrices (Fig. 7C). In normal rats, the connectivity difference between the left SC and the left VP (−0.35) is negative compared to a positive difference of 0.19 in denervated rats. The hypothesis is made that this represents a strengthening of the intrahemispheric connection and a weakening of the interhemispheric connection between these two regions in deafferented rats. The multisensory SC region also exhibits a strengthening of the connection to left S1FL (−0.24 difference) and left M1/M2 (−0.18 difference) when comparing normal and denervated animals. The left hemisphere is contralateral to the denervated right paw, and the hypothesis is made that this represents a strengthening of connectivity between these regions. The hippocampus region in the visual system RPCC matrices (Fig. 8) also shows that the coupling of the right hippocampus to the right SC is altered by denervation by −0.22. Again, the SC is involved in multisensory processing.

Discussion

General discussion

The rat forepaw is innervated by the four major nerves of the brachial plexus: median, ulnar, radial, and musculocutaneous. Each nerve contains both motor and sensory fascicles. In this study, limb deafferentation was performed to disrupt both afferent and efferent signals between the CNS and PNS. It is well known that the size of the cortical representation of a body structure (forelimb, face, etc.) is governed by its degree of sensory innervation (Lee and Woolsey 1975). The whisker field and the forepaw are the largest sensory organs in the rat and, therefore, have the largest cortical brain representations (Paxinos 2004). In this study, it was demonstrated that by transecting the nerves of the forelimb, resting-state BOLD LFFs are disrupted and can be detected with a high-field, small-animal MRI scanner.

Peripheral nerve transection causes cellular remodeling of the brain and spinal cord. (For a review on peripheral nerve injury, please see Navarro et al. [Navarro et al. 2007]). Deafferentation can cause detectable changes in the sensory cortex, which was first demonstrated in a rat by whisker removal (Van der Loos and Woolsey 1973). Reorganization is not limited to the cortex and can involve the thalamus (Kaas 1999; Nicolelis et al. 1993) and other subcortical structures (Lane et al. 2008). Neuroplasticity in the CNS occurs in a time-dependent manner (Cusick 1996) and can include many processes such as the sprouting of new connections or the immediate loss of inhibitory inputs from one region to another (Navarro et al. 2007). Large-scale cellular changes have been shown to occur in response to peripheral nerve injury (Lundborg 2000). It is unknown what neurological processes can alter BOLD LFFs in response to forelimb denervation. Histological studies in different animal models demonstrate neuronal structural changes in the cortex to deafferentation (Navarro et al. 2007). Recently, it was demonstrated that BOLD LFFs are correlated with spontaneous neuronal oscillations detected by electroencephalography (EEG) in animal models (Lu et al. 2007; Shmuel and Leopold 2008). We can make two hypotheses about the causes of changes in the sensorimotor task-activation maps and resting-state RPCC matrices of deafferented rats compared to normal healthy controls. The first hypothesis is that detectable changes in fcMRI maps are due to underlying neuronal activity. The second hypothesis is that the changes in the resting-state maps reflect changes in BOLD neurovascular coupling or plasticity of the microcirculation. Further study is needed to test these hypotheses.

Differences in BOLD fMRI response between normal and denervated rats

Comparing control and experimental animals, Fig. 2 highlights major changes in the task-activated network in response to radial nerve stimulation. There is bilateral negative BOLD activation in the caudate putamen in response to radial nerve stimulation in normal rats. In denervated experimental rats, there is positive BOLD activation in response to nerve stimulation. The caudate region has been implicated in motor planning (Paxinos 2004). Negative BOLD response is still a matter of debate in the fMRI literature. Some groups attribute negative BOLD response to hyper-excitation (Schridde et al. 2008), whereas other groups attribute it to inhibitory input to a given region (Kastrup et al. 2008;Stefanovic et al. 2004). Our data are in agreement with the inhibitory influence hypothesis. Deafferentation causes a loss of inhibitory influence to a given region, which reveals previously inhibited or subthreshold connections. There is a negative BOLD response evident in the S1FL region of healthy animals in the side ipsilateral to stimulation in Fig. 2A. After denervation, a bilateral positive BOLD response to radial nerve stimulation is revealed in Fig. 2C. A similar change in activation pattern occurs in the reticular nuclei of the thalamus in Figs. 2B,D. Contralateral positive BOLD activation occurs in healthy animals in response to radial nerve stimulation (Fig. 2B). After denervation, bilateral positive BOLD activation is observed in the reticular nuclei in response to radial nerve stimulation (Fig. 2D). Previous retrograde labeling experiments in rats have shown that the rostral part of the reticular nucleus projects to the contralateral thalamus (Raos and Bentivoglio 1993). A recent paper has described these contralateral thalamic projections as modulators in rats (Alloway et al. 2008). Our hypothesis is that denervation removes the inhibitory influence from the ipsilateral thalamus revealing a positive BOLD response to nerve stimulation. This work is at an early stage, and without confirmatory evidence from electrophysiological studies, it is difficult to determine from which brain regions the inhibitory influence originates.

Intrahemispheric plasticity

Table 1 shows just a simple statistically significant difference in the known intrahemispheric regional sensorimotor correlations comparing healthy and deafferented rats: left-brain S1FL to M1/M2 (0.49). This is a decrease compared to the other correlation coefficients in that category. The left S1FL is associated with the right deafferented forepaw. The hypothesis is made that a decrease in value represents a weakening of the connectivity between these regions. Several interesting findings have been documented in rats using electrophysiological techniques studying intrahemispheric cortical plasticity that agree with the hypothesis of decreasing connectivity. The cortical representation of the shoulder has been shown to expand into the cortical space formally occupied by the forelimb after limb deafferentation in adult rats (Pearson et al. 2003). It also has been shown that tactile impoverishment, such as placing a cast on a limb for a period of several weeks, causes a reduction in the cortical representation of the paw (Coq and Xerri 1999). These studies support the hypothesis that limb deafferentation causes a weakening of the intrahemispheric connection between S1FL and M1/M2.

Most intrahemispheric electrophysiological studies have focused on the S1FL region, which is possibly due to spatial limitations. MRI has an advantage over electrophysiology in that the entire brain can be studied, including often overlooked subcortical regions. Significant regional intrahemispheric differences are detected in the thalamic nuclei in the current work. For example, the difference in correlations between thalamic nuclei VP to PO is 0.30 for the right hemisphere and 0.15 for the left. There are also statistically significant decreases for intrahemispheric connections that carry multisensory information in the visual system, such as left-hemisphere LP to TeA (0.27) and right-hemisphere SC to LP (0.22). We hypothesize that these lower values represent a weakening of the connections between these multisensory regions in response to limb deafferentation. Further studies with multimodal approaches will be necessary (*i.e.*, combined resting-state EEG with fcMRI).

Interhemispheric plasticity

Bilateral cortical reorganization in response to deafferentation was first demonstrated by Calford and Tweedale (Calford and Tweedale 1990). They demonstrated that cross-hemispheric plasticity was brought about by digit amputation in flying foxes. In the current study, we examined known cross-hemispheric cortical connections, which are listed in Fig. 6. These correlation values are then displayed in Fig. 9. There are statistically significant decreases in value between the cross-hemispheric cortical connections (M1/M2, S1, S2) when healthy rats are contrasted to deafferented rats. These results are in agreement with two recent studies looking at cross-cortical connections using fcMRI in human subjects (Johnston et al. 2008; Uddin et al. 2008). Both studies compared the interhemispheric network connectivity between healthy controls and subjects that underwent "split brain" procedures to relieve severe epilepsy. The researchers found that by surgical transection of the corpus callosum, the cross-hemispheric connectivity was diminished (Uddin et al. 2008) or absent (Johnston et al. 2008).

In the case of diminishment, the investigators hypothesized that the remaining interhemispheric connectivity was due to subcortical interhemispheric connection. In the current work, an interhemispheric subcortical connection is revealed in the task-activated network. There is single-sided activation in the reticular thalamic nuclei in the hemisphere contralateral to direct radial nerve stimulation in healthy rats (Fig. 2D) and bilateral hemispheric activation in response to radial nerve stimulation of the healthy limb in deafferented subjects. The reticular nuclei have been shown to be connected across brain hemispheres in the rat (Chen et al. 1992;Raos and Bentivoglio 1993). Difference in cross-hemispheric connections can also be demonstrated for the thalamic (SMT, VP, PO) interhemispheric connectivities in the sensorimotor system by examining the difference map (Fig. 7C). If the same examination is done for the difference map in the visual system (Fig. 8C), only areas that carry multisensory information (TeA, LP, SC) demonstrate cross-hemispheric differences. This is a key finding in this work and reveals the value of fcMRI in the study of neuroplasticity.

Our activated fMRI data are in fair agreement with a previous rat study of forepaw denervation and BOLD fMRI (Pelled et al. 2007). These investigators denervated a single forepaw by cutting the median, ulnar, and radial nerves, but not the musculocutaneous nerve, in juvenile rats. By BOLD fMRI they detected bilateral cortical S1FL activation in response to electrical forepaw stimulation to the intact forelimb, as determined in this study by direct radial nerve stimulation. Bilateral activation in response to sensory stimulation of the healthy forepaw in limb amputation has also been demonstrated using electrophysiological means in neonatal rats (Pluto et al. 2005). Pelled et al. (Pelled et al. 2007) found that cross-hemispheric reorganization occurs through an intercortical pathway and hypothesized that cross-hemispheric inhibition is responsible for the normal suppression of the bilateral response. The current study differs from these studies (Pelled et al. 2007; Pluto et al. 2005) in that adult rather than juvenile rats were studied. Cortical and subcortical reorganization following limb deafferentation has been shown to be different if the injury occurs in the adult or neonatal stage (Bowlus et al. 2003; Pearson et al. 1999). Our inability to detect changes in the task-activated network in the forepaw stimulation experiments may be due to the age of the animals in our study, the anesthetic used, or the robustness of the forepaw stimulus used in the previous study (Pelled et al. 2007).

fMRI vs. fcMRI

It was first hypothesized by Xiong et al. (Xiong et al. 1999) that the task-activated fMRI network is a subset of the resting-state network. In this study, electrical forepaw stimulation is one of the experimental tasks used. Rat forepaw stimulation, which has been used since the early development of fMRI (Hyder et al. 1994), mainly activates the somatosensory forelimb region (S1FL) in the brain, with little subcortical activation (Keilholz et al. 2004). It is

technically challenging to design a motor task for anesthetized animals within the scanner environment. Direct nerve stimulation in rats activates motor, sensory, and subcortical regions and is a viable alternative to motor task activation(Cho et al. 2007).

In denervated animals, devising a task is not possible because the nerves to the area of interest have been transected, but fcMRI is feasible. In the fcMRI analysis, brain regions are selected based on areas considered to be part of the sensorimotor system in prior fMRI experiments or drawn from consultation with the rat brain atlas (Paxinos 2005). Both cortical and subcortical structures can be included and regional correlations in BOLD LFFs tested. In fcMRI, the entire network is tested for neuroplastic changes in the connections between regions, whereas in fMRI, only the task-activated network can be analyzed. This work supports the hypothesis that fMRI and fcMRI together provide a general marker for brain plasticity.

The use of fcMRI in the study of neuroplasticity

Recently, fcMRI has been applied to the study of the developing child brain (Fair et al. 2008; Fransson et al. 2007). These studies on children (Fair et al. 2008; Fransson et al. 2007) demonstrate that the correlations in BOLD LFFs between brain systems are disordered in the very young and become more correlated with increasing age. Fransson et al. (Fransson et al. 2007) demonstrated that interhemispheric functional connectivity was stronger than intrahemispheric connectivity in infant subjects. It has been shown that white matter tracts are more developed across cortical hemispheres than in the anterior-to-posterior direction (Dubois 2008). In this work, the strongest changes that were observed with fMRI following peripheral nerve transection were interhemispheric. Based on this observation, it appears that fcMRI will be useful in studying the time-dependence of CNS remodeling following nerve injury. Further studies are warranted in animal models and may be possible in humans who have had limb amputation or other peripheral nerve injuries.

Conclusion

This work demonstrates that the loss of afferent input causes detectable changes in the correlations in resting-state BOLD LFFs between regions of the fMRI task network. Distinguishing changes in the task-activated network required using a more invasive task (direct nerve stimulation). Functional connectivity MRI has utility over fMRI in studying injury in cases where design of a task is problematic. Here, we establish for the first time that lesional changes in the PNS cause changes in the baseline or resting-state brain. These changes can be identified by fcMRI and used as a marker for neuroplasticity.

Acknowledgments

This work was supported by grants EB000215, EB000215-S1, and GM56398 from the National Institutes of Health, and DABK39-03-C-0058 from the Counterdrug Technology Assessment Center, Office of National Drug Control Policy, White House. The authors would also like to thank Abbie Amadio and Karen Hyde for figure preparation and manuscript editing.

References

Alloway KD, Olson ML, Smith JB. Contralateral corticothalamic projections from MI whisker cortex: Potential route for modulating hemispheric interactions. J Comp Neurol 2008;510:100–116. [PubMed: 18615539]

Biswal B, Yetkin FZ, Haughton VM, Hyde JS. Functional connectivity in the motor cortex of resting human brain using echo-planar MRI. Magn Reson Med 1995;34:537–541. [PubMed: 8524021]

Bowlus TH, Lane RD, Stojic AS, Johnston M, Pluto CP, Chan M, Chiaia NL, Rhoades RW. Comparison of reorganization of the somatosensory system in rats that sustained forelimb removal as neonates and as adults. J Comp Neurol 2003;465:335–348. [PubMed: 12966559]

Calford MB, Tweedale R. Interhemispheric transfer of plasticity in the cerebral cortex. Science 1990;249:805–807. [PubMed: 2389146]

Chen S, Raos V, Bentivoglio M. Connections of the thalamic reticular nucleus with the contralateral thalamus in the rat. Neurosci Lett 1992;147:85–88. [PubMed: 1480329]

Cho YR, Pawela CP, Li R, Kao D, Schulte ML, Runquist ML, Yan JG, Matloub HS, Jaradeh SS, Hudetz AG, Hyde JS. Refining the sensory and motor ratunculus of the rat upper extremity using fMRI and direct nerve stimulation. Magn Reson Med 2007;58:901–909. [PubMed: 17969116]

Coq JO, Xerri C. Tactile impoverishment and sensorimotor restriction deteriorate the forepaw cutaneous map in the primary somatosensory cortex of adult rats. Exp Brain Res 1999;129:518–531. [PubMed: 10638426]

Cox RW, Hyde JS. Software tools for analysis and visualization of fMRI data. NMR Biomed 1997;10:171–178. [PubMed: 9430344]

Cusick CG. Extensive cortical reorganization following sciatic nerve injury in adult rats versus restricted reorganization after neonatal injury: Implications for spatial and temporal limits on somatosensory plasticity. Prog Brain Res 1996;108:379–390. [PubMed: 8979815]

Donoghue JP, Sanes JN. Peripheral nerve injury in developing rats reorganizes representation pattern in motor cortex. Proc Natl Acad Sci USA 1987;84:1123–1126. [PubMed: 3469649]

Donoghue JP, Sanes JN. Organization of adult motor cortex representation patterns following neonatal forelimb nerve injury in rats. J Neurosci 1988;8:3221–3232. [PubMed: 3171676]

Dubois JDLG, Perrin M, Mangin JF, Cointepas Y, Duchesnay E, Le Bihan D, Hertz-Pannier L. Asynchrony of the early maturation of white matter bundles in healthy infants: quantitative landmarks revealed noninvasively by diffusion tensor imaging. Hum Brain Mapp 2008;29:14–27. [PubMed: 17318834]

Endo T, Spenger C, Tominaga T, Brene S, Olson L. Cortical sensory map rearrangement after spinal cord injury: fMRI responses linked to Nogo signaling. Brain 2007;130:2951–2961. [PubMed: 17913768]

Fair DA, Cohen AL, Dosenbach NU, Church JA, Miezin FM, Barch DM, Raichle ME, Petersen SE, Schlaggar BL. The maturing architecture of the brain's default network. Proc Natl Acad Sci USA 2008;105:4028–4032. [PubMed: 18322013]

Feydy A, Carlier R, Roby-Brami A, Bussel B, Cazalis F, Pierot L, Burnod Y, Maier MA. Longitudinal study of motor recovery after stroke: recruitment and focusing of brain activation. Stroke 2002;33:1610–1617. [PubMed: 12053000]

Fox MD, Raichle ME. Spontaneous fluctuations in brain activity observed with functional magnetic resonance imaging. Nat Rev Neurosci 2007;8:700–711. [PubMed: 17704812]

Fransson P, Skiold B, Horsch S, Nordell A, Blennow M, Lagercrantz H, Aden U. Resting-state networks in the infant brain. Proc Natl Acad Sci USA 2007;104:15531–15536. [PubMed: 17878310]

Greicius MD, Krasnow B, Reiss AL, Menon V. Functional connectivity in the resting brain: A network analysis of the default mode hypothesis. Proc Natl Acad Sci USA 2003;100:253–258. [PubMed: 12506194]

Hyder F, Behar KL, Martin MA, Blamire AM, Shulman RG. Dynamic magnetic resonance imaging of the rat brain during forepaw stimulation. J Cereb Blood Flow Metab 1994;14:649–655. [PubMed: 8014212]

Jenkinson M, Smith S. A global optimisation method for robust affine registration of brain images. Med Image Anal 2001;5:143–156. [PubMed: 11516708]

Johnston JM, Vaishnavi SN, Smyth MD, Zhang D, He BJ, Zempel JM, Shimony JS, Snyder AZ, Raichle ME. Loss of resting interhemispheric functional connectivity after complete section of the corpus callosum. J Neurosci 2008;28:6453–6458. [PubMed: 18562616]

Kaas JH. Is most of neural plasticity in the thalamus cortical? Proc Natl Acad Sci USA 1999;96:7622–7623. [PubMed: 10393868]

Kalaska J, Pomeranz B. Chronic paw denervation causes an age-dependent appearance of novel responses from forearm in "paw cortex" of kittens and adult cats. J Neurophysiol 1979;42:618–633. [PubMed: 422979]

Kannurpatti SS, Biswal BB, Kim YR, Rosen BR. Spatio-temporal characteristics of low-frequency BOLD signal fluctuations in isoflurane-anesthetized rat brain. Neuroimage 2008;40:1738–1747. [PubMed: 18339559]

Karni A, Meyer G, Jezzard P, Adams MM, Turner R, Ungerleider LG. Functional MRI evidence for adult motor cortex plasticity during motor skill learning. Nature 1995;377:155 –158. [PubMed: 7675082]

Kastrup A, Baudewig J, Schnaudigel S, Huonker R, Becker L, Sohns JM, Dechent P, Klingner C, Witte OW. Behavioral correlates of negative BOLD signal changes in the primary somatosensory cortex. Neuroimage 2008;41:1364–1371. [PubMed: 18495495]

Keilholz SD, Silva AC, Raman M, Merkle H, Koretsky AP. Functional MRI of the rodent somatosensory pathway using multislice echo planar imaging. Magn Reson Med 2004;52:89–99. [PubMed: 15236371]

Lane RD, Pluto CP, Kenmuir CL, Chiaia NL, Mooney RD. Does reorganization in the cuneate nucleus following neonatal forelimb amputation influence development of anomalous circuits within the somatosensory cortex? J Neurophysiol 2008;99:866–875. [PubMed: 18032566]

Lee KJ, Woolsey TA. A proportional relationship between peripheral innervation density and cortical neuron number in the somatosensory system of the mouse. Brain Res 1975;99:349–353. [PubMed: 1182550]

Li SJ, Li Z, Wu G, Zhang MJ, Franczak M, Antuono PG. Alzheimer's disease: Evaluation of a functional MR imaging index as a marker. Radiology 2002;225:253–259. [PubMed: 12355013]

Liu Y, Liang M, Zhou Y, He Y, Hao Y, Song M, Yu C, Liu H, Liu Z, Jiang T. Disrupted small-world networks in schizophrenia. Brain 2008;131:945–961. [PubMed: 18299296]

Liu Y, Yu C, Liang M, Li J, Tian L, Zhou Y, Qin W, Li K, Jiang T. Whole brain functional connectivity in the early blind. Brain 2007;130:2085–2096. [PubMed: 17533167]

Lu H, Zuo Y, Gu H, Waltz JA, Zhan W, Scholl CA, Rea W, Yang Y, Stein EA. Synchronized delta oscillations correlate with the resting-state functional MRI signal. Proc Natl Acad Sci USA 2007;104:18265–18269. [PubMed: 17991778]

Lundborg G. Brain plasticity and hand surgery: An overview. J Hand Surg [Br] 2000;25:242–252.

Merzenich MM, Kaas JH, Wall J, Nelson RJ, Sur M, Felleman D. Topographic reorganization of somatosensory cortical areas 3b and 1 in adult monkeys following restricted deafferentation. Neuroscience 1983a;8:33–55. [PubMed: 6835522]

Merzenich MM, Kaas JH, Wall JT, Sur M, Nelson RJ, Felleman DJ. Progression of change following median nerve section in the cortical representation of the hand in areas 3b and 1 in adult owl and squirrel monkeys. Neuroscience 1983b;10:639–665. [PubMed: 6646426]

Navarro X, Vivo M, Valero-Cabre A. Neural plasticity after peripheral nerve injury and regeneration. Prog Neurobiol 2007;82:163–201. [PubMed: 17643733]

Nicolelis MA, Lin RC, Woodward DJ, Chapin JK. Induction of immediate spatiotemporal changes in thalamic networks by peripheral block of ascending cutaneous information. Nature 1993;361:533–536. [PubMed: 8429906]

Pawela CP, Biswal BB, Cho YR, Kao DS, Li R, Jones SR, Schulte ML, Matloub HS, Hudetz AG, Hyde JS. Resting-state functional connectivity of the rat brain. Magn Reson Med 2008;59:1021–1029. [PubMed: 18429028]

Paxinos, G. The Rat Nervous System. New York: Academic Press; 2004.

Paxinos, G.; Watson, C. The Rat Brain in Stereotaxic Coordinates. New York: Elsevier Academic Press; 2005.

Pearson PP, Li CX, Chappell TD, Waters RS. Delayed reorganization of the shoulder representation in forepaw barrel subfield (FBS) in first somatosensory cortex (SI) following forelimb deafferentation in adult rats. Exp Brain Res 2003;153:100–112. [PubMed: 12955377]

Pearson PP, Li CX, Waters RS. Effects of large-scale limb deafferentation on the morphological and physiological organization of the forepaw barrel subfield (FBS) in somatosensory cortex (SI) in adult and neonatal rats. Exp Brain Res 1999;128:315–331. [PubMed: 10501804]

Pelled G, Chuang KH, Dodd SJ, Koretsky AP. Functional MRI detection of bilateral cortical reorganization in the rodent brain following peripheral nerve deafferentation. Neuroimage 2007;37:262–273. [PubMed: 17544301]

Pelled G, Dodd SJ, Koretsky AP. Catheter confocal fluorescence imaging and functional magnetic resonance imaging of local and systems level recovery in the regenerating rodent sciatic nerve. Neuroimage 2006;30:847–856. [PubMed: 16343952]

Pluto CP, Chiaia NL, Rhoades RW, Lane RD. Reducing contralateral SI activity reveals hindlimb receptive fields in the SI forelimb-stump representation of neonatally amputated rats. J Neurophysiol 2005;94:1727–1732. [PubMed: 15800076]

Pons TP, Garraghty PE, Ommaya AK, Kaas JH, Taub E, Mishkin M. Massive cortical reorganization after sensory deafferentation in adult macaques. Science 1991;252:1857–1860. [PubMed: 1843843]

Raichle ME, Snyder AZ. A default mode of brain function: A brief history of an evolving idea. Neuroimage 2007;37:1083–1090. discussion 1097–1099. [PubMed: 17719799]

Ramu J, Bockhorst KH, Grill RJ, Mogatadakala KV, Narayana PA. Cortical reorganization in NT3-treated experimental spinal cord injury: Functional magnetic resonance imaging. Exp Neurol 2007;204:58–65. [PubMed: 17112518]

Raos V, Bentivoglio M. Crosstalk between the two sides of the thalamus through the reticular nucleus: A retrograde and anterograde tracing study in the rat. J Comp Neurol 1993;332:145–154. [PubMed: 8331209]

Sanes JN, Suner S, Donoghue JP. Dynamic organization of primary motor cortex output to target muscles in adult rats. I Long-term patterns of reorganization following motor or mixed peripheral nerve lesions. Exp Brain Res 1990;79:479–491. [PubMed: 2340868]

Sanes JN, Suner S, Lando JF, Donoghue JP. Rapid reorganization of adult rat motor cortex somatic representation patterns after motor nerve injury. Proc Natl Acad Sci USA 1988;85:2003–2007. [PubMed: 3162322]

Schridde U, Khubchandani M, Motelow JE, Sanganahalli BG, Hyder F, Blumenfeld H. Negative BOLD with large increases in neuronal activity. Cereb Cortex 2008;18:1814–1827. [PubMed: 18063563]

Shmuel A, Leopold DA. Neuronal correlates of spontaneous fluctuations in fMRI signals in monkey visual cortex: Implications for functional connectivity at rest. Hum Brain Mapp 2008;29:751–761. [PubMed: 18465799]

Sorg C, Riedl V, Muhlau M, Calhoun VD, Eichele T, Laer L, Drzezga A, Forstl H, Kurz A, Zimmer C, Wohlschlager AM. Selective changes of resting-state networks in individuals at risk for Alzheimer's disease. Proc Natl Acad Sci USA 2007;104:18760–18765. [PubMed: 18003904]

Stefanovic B, Warnking JM, Pike GB. Hemodynamic and metabolic responses to neuronal inhibition. Neuroimage 2004;22:771–778. [PubMed: 15193606]

Uddin LQ, Mooshagian E, Zaidel E, Scheres A, Margulies DS, Kelly AM, Shehzad Z, Adelstein JS, Castellanos FX, Biswal BB, Milham MP. Residual functional connectivity in the split-brain revealed with resting-state functional MRI. Neuroreport 2008;19:703–709. [PubMed: 18418243]

Van der Loos H, Woolsey TA. Somatosensory cortex: Structural alterations following early injury to sense organs. Science 1973;179:395–398. [PubMed: 4682966]

Vincent JL, Patel GH, Fox MD, Snyder AZ, Baker JT, Van Essen DC, Zempel JM, Snyder LH, Corbetta M, Raichle ME. Intrinsic functional architecture in the anaesthetized monkey brain [see comment]. Nature 2007;447:83–86. [PubMed: 17476267]

Wall JT, Cusick CG. Cutaneous responsiveness in primary somatosensory (S-I) hindpaw cortex before and after partial hindpaw deafferentation in adult rats. J Neurosci 1984;4:1499–1515. [PubMed: 6726345]

Wall JT, Cusick CG. The representation of peripheral nerve inputs in the S-I hindpaw cortex of rats raised with incompletely innervated hindpaws. J Neurosci 1986;6:1129–1147. [PubMed: 3701411]

Weber R, Ramos-Cabrer P, Justicia C, Wiedermann D, Strecker C, Sprenger C, Hoehn M. Early prediction of functional recovery after experimental stroke: Functional magnetic resonance imaging, electrophysiology, and behavioral testing in rats. J Neurosci 2008;28:1022–1029. [PubMed: 18234880]

Xiong J, Parsons LM, Gao JH, Fox PT. Interregional connectivity to primary motor cortex revealed using MRI resting state images. Hum Brain Mapp 1999;8:151–156. [PubMed: 10524607]

Zhao F, Zhao T, Zhou L, Wu Q, Hu X. BOLD study of stimulation-induced neural activity and resting-state connectivity in medetomidine-sedated rat. Neuroimage 2008;39:248–260. [PubMed: 17904868]

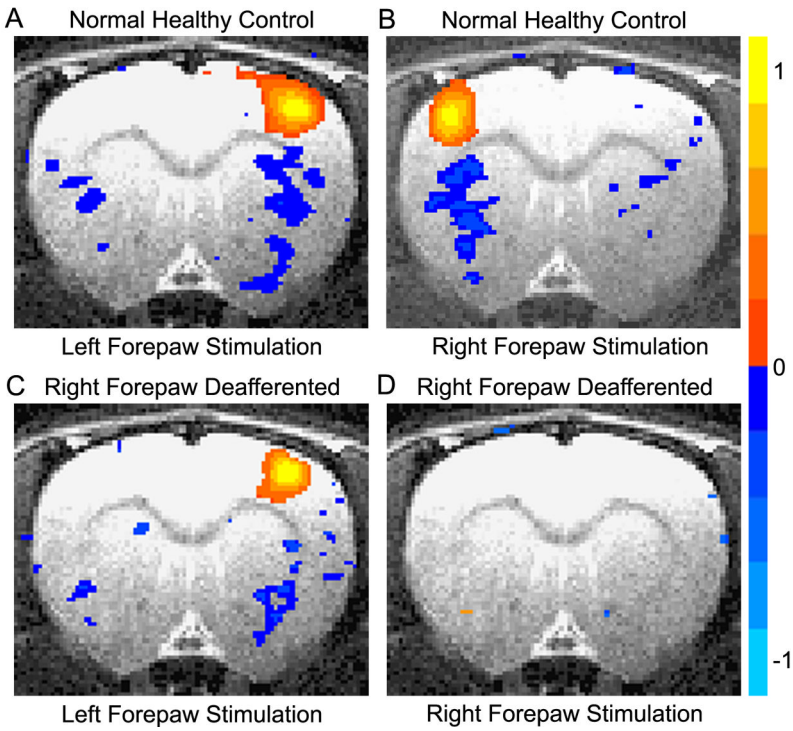

Fig. 1.

Functional averaged activation map resulting from electrical forepaw stimulation. (A) Left-paw stimulation in six healthy rats. (B) Right-paw stimulation in six healthy rats. (C) Left-paw stimulation in six right-paw-deafferented rats. (D) Right-paw stimulation in six right-paw-deafferented rats. Stimulation parameters were 2 mA, 3 ms, and 10 Hz. A p-value of 0.005 was the threshold used for plotting. The color bar displays task correlation from −1.0 to 1.0.

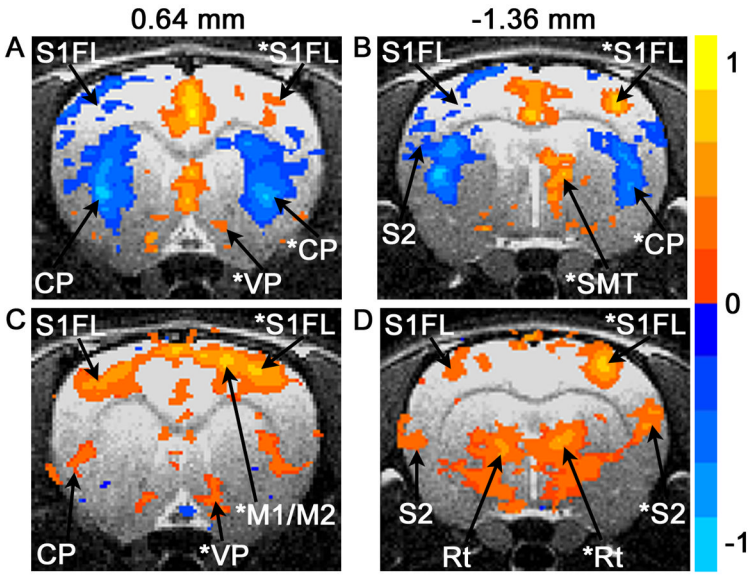

Fig. 2.

Functional activation map in response to direct radial nerve stimulation. (A, B) Direct radial nerve stimulation to left limb in six healthy rats. (C, D) Direct radial nerve stimulation to left limb in six right-side-deafferented rats. (A, C) Slice centered 0.64 mm from bregma. (B, D) Slice centered −1.36 mm from bregma. Stimulation parameters were 1 mA, 1 ms, and 5 Hz. A p-value of 0.005 was the threshold used for plotting. An asterisk (*) indicates the hemisphere contralateral to simulation. The color bar displays task correlation from −1.0 to 1.0. See Material and Methods for abbreviations.

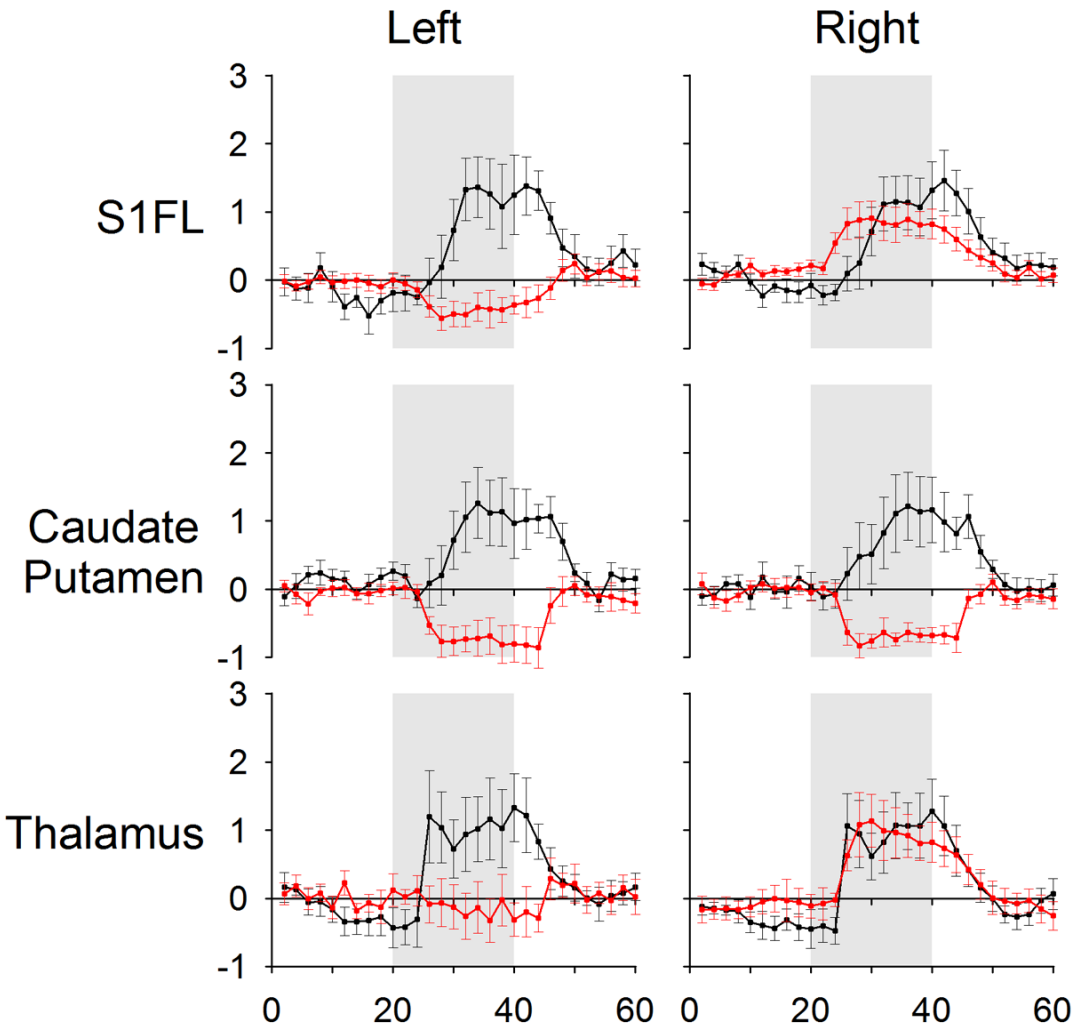

Fig. 3.

Percent signal change in response to direct radial nerve stimulation. Time-courses averaged across both deafferented (black) and healthy control (red) rats. Activated voxels originated in three different regions of the sensorimotor system. Stimulation parameters were 1 mA, 1 ms, and 5 Hz. A p-value of 0.005 was the threshold considered for activation. Error bars indicate standard error of the mean.

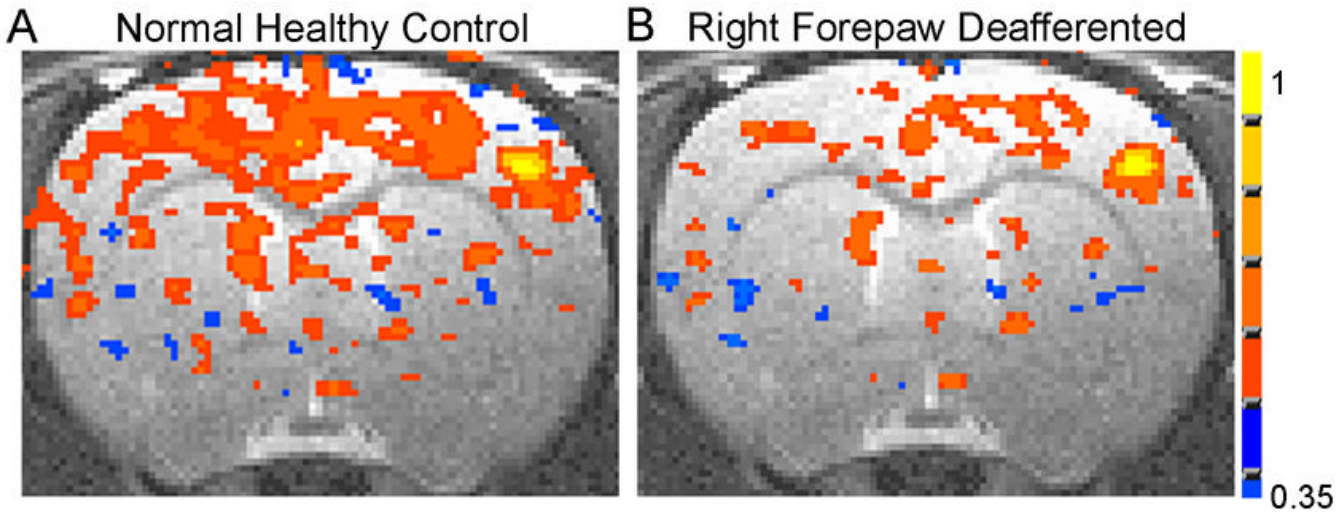

Fig. 4.

Resting-state fcMRI seed voxel correlation maps. (A) Map generated from a normal healthy rat. (B) Map generated from a deafferented rat. Seed region located in the right S1FL region (ipsilateral to the right denervated forelimb in the experimental animals). The seed region has the highest correlation and is shown in yellow. Presented slice located −0.64 mm from bregma. The color bar displays correlation coefficient strength from 0.35 to 1.0.

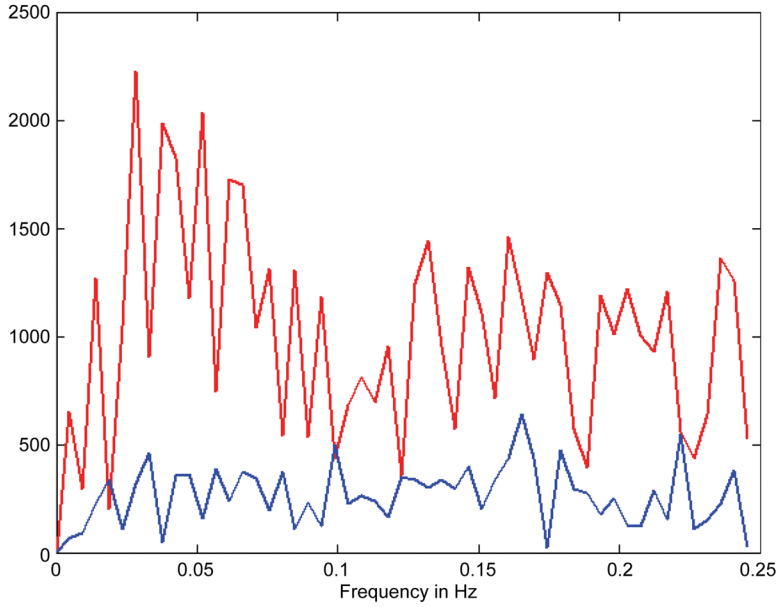

Fig. 5.

Power spectra from regional resting-state time-courses. Power vs. frequency in hertz is plotted. The blue spectrum was created by using a region located outside the brain. The red spectrum was created using a representative region used in the PCA analysis.

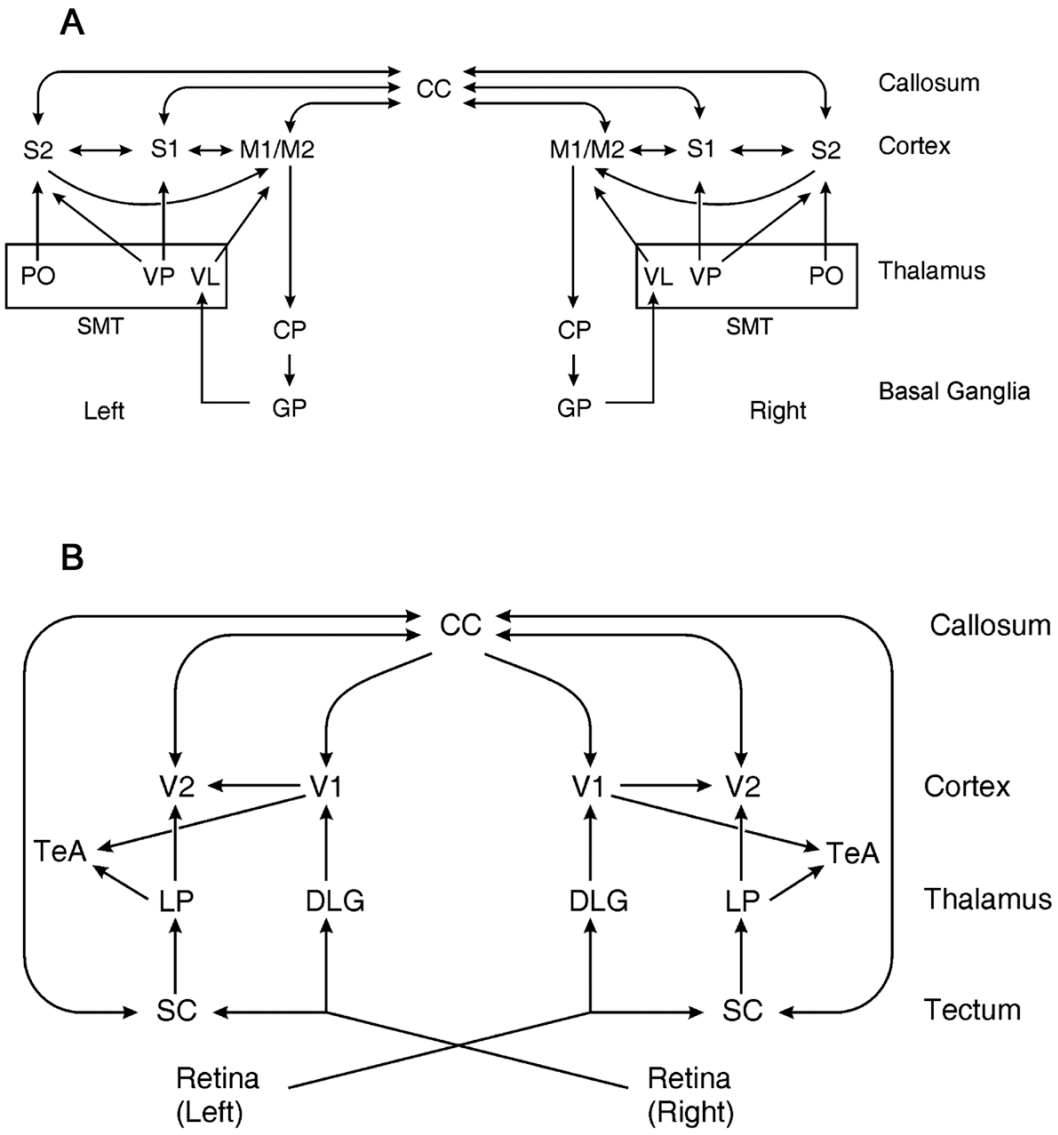

Fig. 6.

Simplified connection flowcharts of the rodent brain networks determined by prior studies. (A) Rodent sensorimotor system. (B) Rodent visual system. System hierarchy moves from top to bottom. Arrows indicate primary information flow in the low to high hierarchy, although reciprocal connections are usually present.

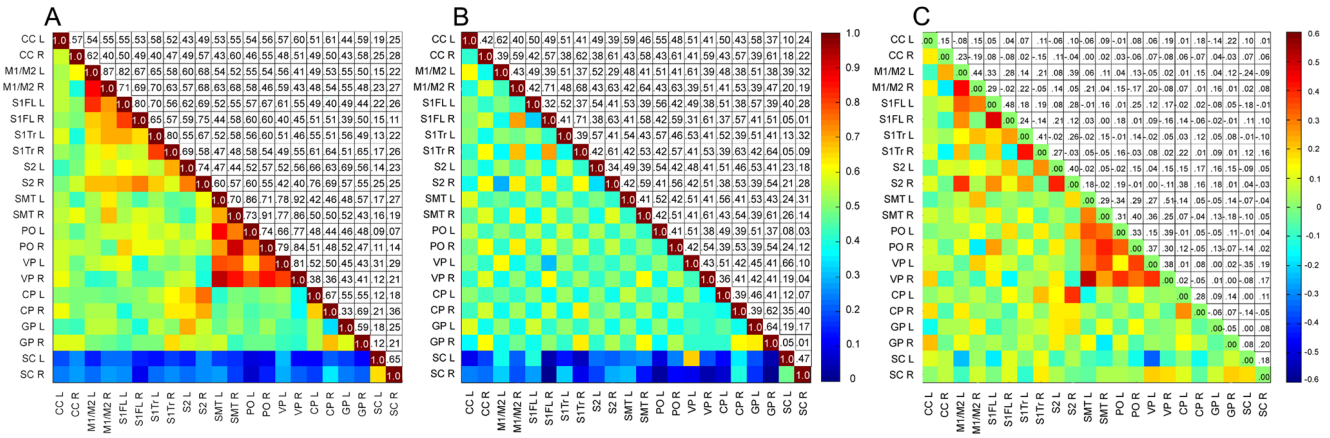

Fig. 7.

RPCC matrices of average resting-state BOLD time-courses in the rat motor/sensory system. (A) RPCC matrix from average of 20 healthy rats. (B) RPCC matrix from average of six animals that received a surgical procedure to denervate the right forepaw. Both the left and right sides of each region were tabulated. The superior colliculus (SC) from the visual system was included as a control. The lower triangular part of the graph displays the coefficient values according to the color bar located between Figs. 7B and 7C, and the upper triangular part (mirror image) of the graph tabulates the corresponding correlation coefficient values. (C) Difference matrix resulting from subtraction of Fig. 7B from Fig. 7A. The lower triangular part of the difference matrix displays the coefficient values according to the color bar on the far right, and the upper triangular part (mirror image) of the graph tabulates the corresponding correlation coefficient differences between Figs. 7A and 7B. A difference of > 0.2 corresponds to a p-value of approximately 0.001 (unpaired t-test). See Material and Methods for abbreviations.

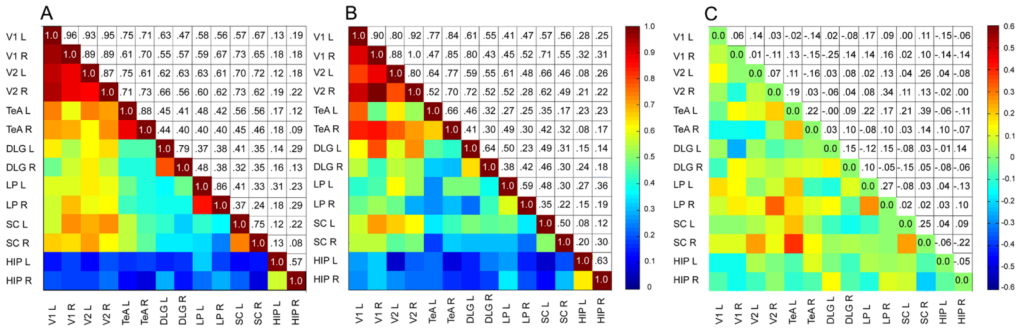

Fig. 8.

RPCC matrices of average resting-state BOLD time-courses in the rat visual system. (A) RPCC matrix from average of 15 healthy rats. (B) RPCC matrix from average of six animals that received a surgical procedure to denervate the right forepaw. Both the left and right sides of each region were tabulated. The hippocampus (HIP) was included as a control. The lower triangular part of the graph displays the coefficient values according to the color bar located between Figs. 8B and 8C, and the upper triangular part (mirror image) of the graph tabulates the corresponding correlation coefficient values. (C) Difference matrix resulting from subtraction of Fig. 8B from Fig. 8A. The lower triangular part of the difference matrix displays the coefficient values according to the color bar on the far right, and the upper triangular part (mirror image) of the graph tabulates the corresponding correlation coefficient differences between Figs. 8A and 8B. A difference of > 0.2 corresponds to a p-value of approximately 0.001 (unpaired t-test). See Materials and Methods for abbreviations.

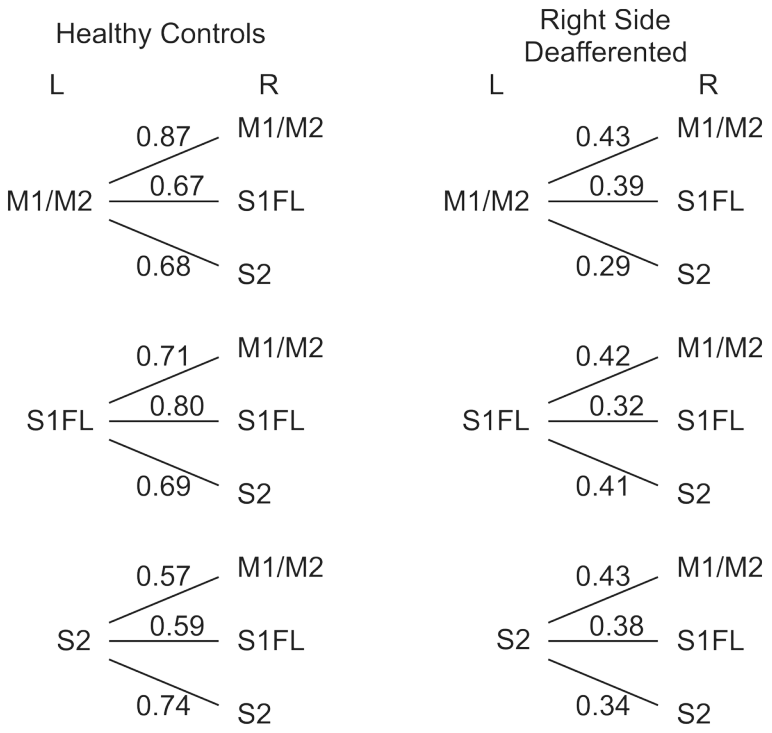

Fig. 9.

Interhemispheric resting-state BOLD fcMRI correlation coefficients between cortical brain regions. Cross-hemispheric connections for both healthy and right-limb-deafferented rats are listed. All differences between matched connections between experimental groups are statistically significant when tested with an unpaired t-test with a 95% confidence interval.

Table 1

Regional Intrahemispheric Brain Connectivities

	Sensorimotor System			
	Healthy Controls		**Right Side Deafferented**	
	Left	**Right**	**Left**	**Right**
S1FL → S2	0.62	0.75	0.54	0.63
S1FL → M1/M2	0.82	0.69	0.49	0.71
S1FL → CC	0.55	0.49	0.50	0.57
S2 → CC	0.43	0.57	0.49	0.61
M1/M2 → CC	0.54	0.40	0.62	0.59
S2 → M1/M2	0.60	0.68	0.63	0.52
PO → S2	0.52	0.55	0.54	0.56
VP → S1FL	0.61	0.45	0.49	0.51
VP → S2	0.52	0.40	0.48	0.51
VL → M1/M2	0.54	0.68	0.48	0.64
M1/M2 → CP	0.49	0.54	0.48	0.53
CP → GP	0.55	0.69	0.46	0.62
GP → VL	0.48	0.43	0.53	0.61
	Visual System			
	Healthy Controls		Right Side Deafferented	
	Left	Right	Left	Right
V1 → V2	0.93	0.89	0.80	1.00
V1 → TeA	0.75	0.70	0.77	0.85
DLG → V1	0.63	0.57	0.61	0.43
LP → V2	0.63	0.62	0.61	0.28
LP → TeA	0.48	0.40	0.27	0.30
SC → LP	0.41	0.35	0.48	0.22

* Highlighted regions indicate statistical significance.